Supporting Information:

Mechanical force-driven multi-state memory in $WO_{3-\delta}$ thin films

Mingdi Yang[1], Zonglin Lv[1], Shan Li[1], Jiaqi Li[1], Jinpeng Cao[1], Junjie Chen[1], Yilin Wang[2], Kun Lin[1], Qiang Li[1]*, Jun Miao[1], Xianran Xing[1]*

[1] *Beijing Advanced Innovation Center for Materials Genome Engineering, Institute of Solid State Chemistry, Department of Physical Chemistry, University of Science and Technology Beijing, Beijing 100083, China*

[2]*College of Materials Science and Engineering, Nanjing Tech University, 30 South Puzhu Road, Nanjing 211816, China*

**Corresponding author:* xing@ustb.edu.cn, qiangli@ustb.edu.cn

09 July 2024

Note added after first publication: This supplementary information file replaces that originally published on 28 May 2024. Figure S4 has been replaced with an updated version with corrected slope values.

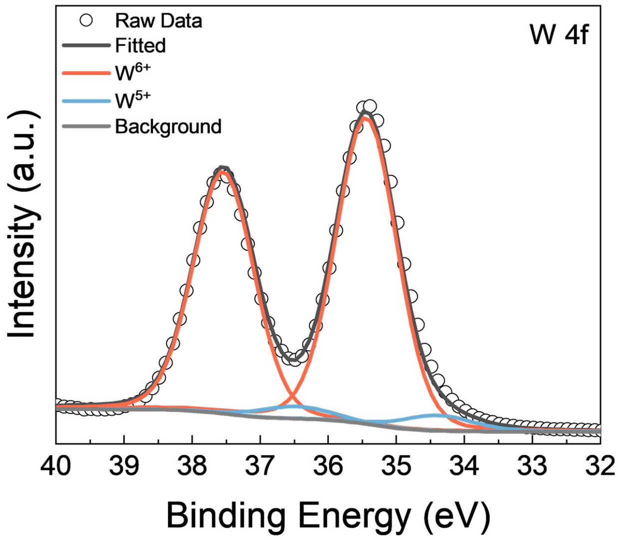

Fig.S1 XPS of W 4f

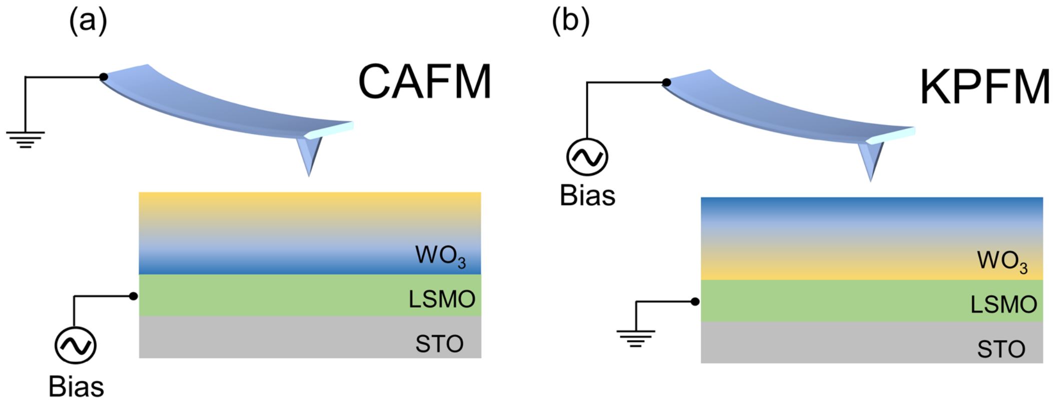

Fig.S2 (a) (b) Schematic diagram of CAFM and KPFM.

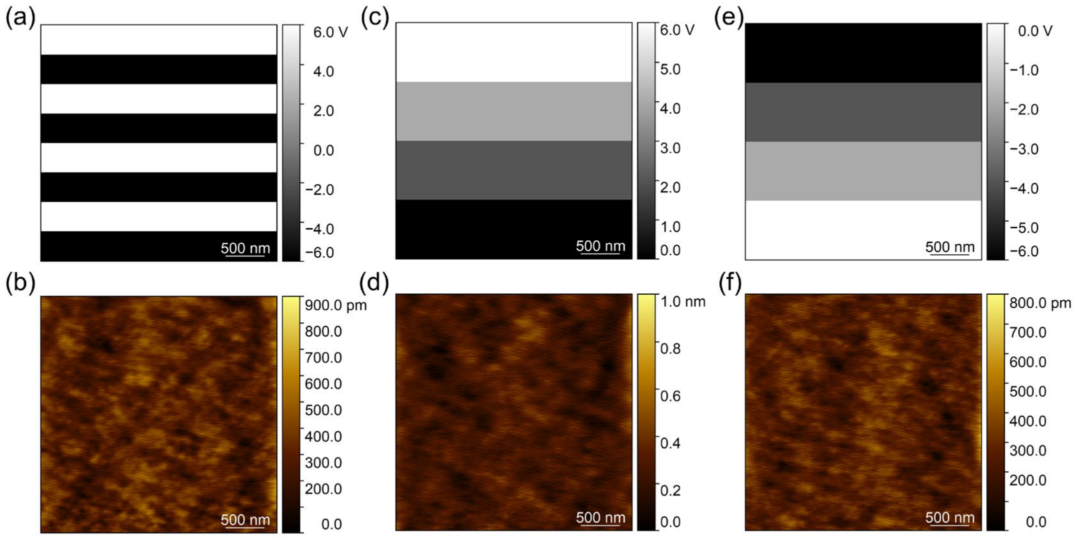

Fig.S3 (a) (c) (e) Applied different voltage for Multilevel storage. (b) (d) (f) Corresponding surface morphology.

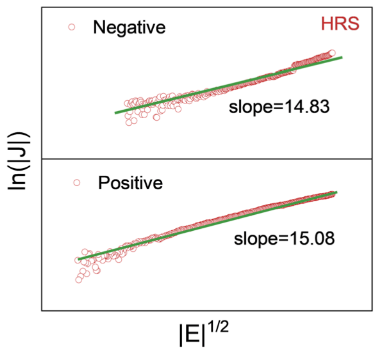

Fig.S4 Schottky emission fitting from *I*-*V* curves of HRS modulated by electrical stimulation.

Taking into account the model and parameters of the chosen diamond probe, as well as the position of the light spot at the probe tip, it is equivalent to applying a force of 5.4 μN on the surface of the $WO_{3-\delta}$ thin film when using a 1 V voltage to perform the written process after experimental calibration and calculation.

$$F = k \cdot \Delta z \tag{1}$$

$$\Delta z = \text{Deflection InvOLS} \cdot \Delta V \tag{2}$$

$$\text{Kappa factor} = \frac{Amplitude\ InvOLS}{Deflection\ InvOLSv} \tag{3}$$

F represents the force along the vertical direction, k (Spring Constant) and Amplitude InvOLS are about 39.84 nN/nm and 147.19 nm/V after calibration, respectively, Kappa factor is about 1.09.

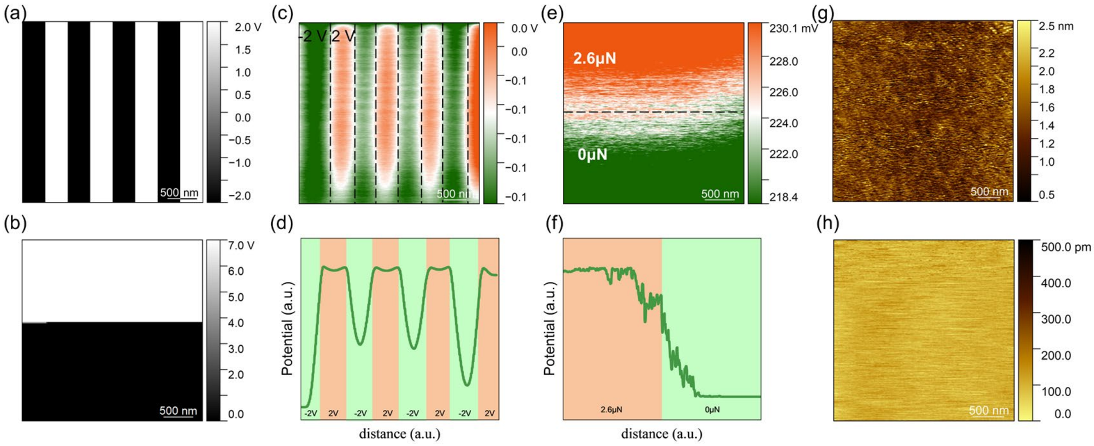

Fig.S5 (a) (b) Applied different voltage and fore for KPFM. (c) (d) KPFM plot after different voltage or mechanical force applied. (e) (f) Corresponding potential statistics chart. (g) (h) Corresponding surface morphology.

In contrast to CAFM measurements, it should be emphasized that voltage is applied through the probe and the bottom electrode is grounded during KPFM measurements (Fig. S1b). The potential that reflects the contact potential difference (CPD) is higher in the region written by +2 V than the region written by -2 V. Likewise, the mechanical force drives various surface potential.

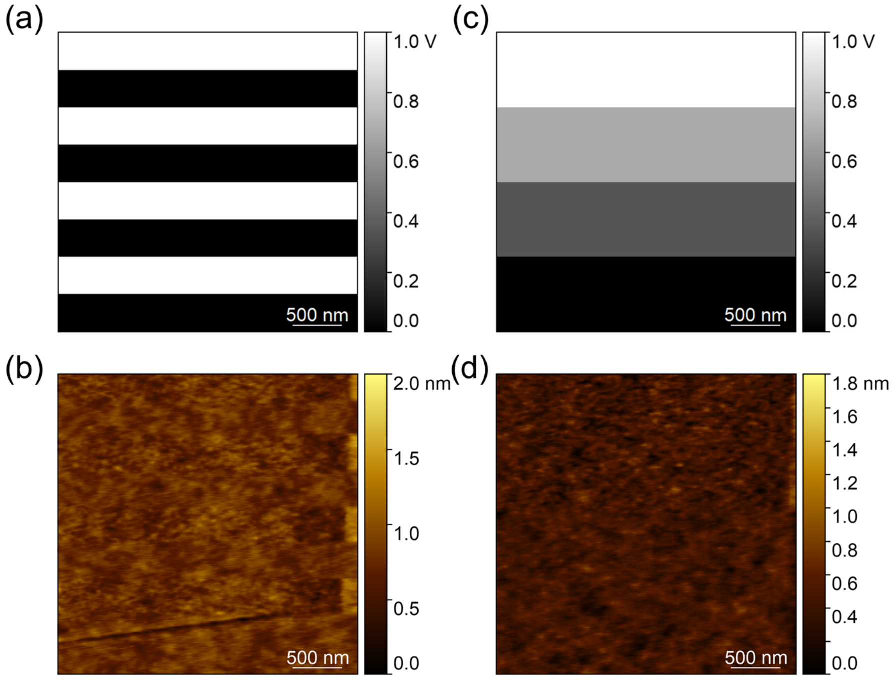

Fig.S6 (a) (c) Applied different forces for Multilevel storage. (b) (d) Corresponding surface morphology.

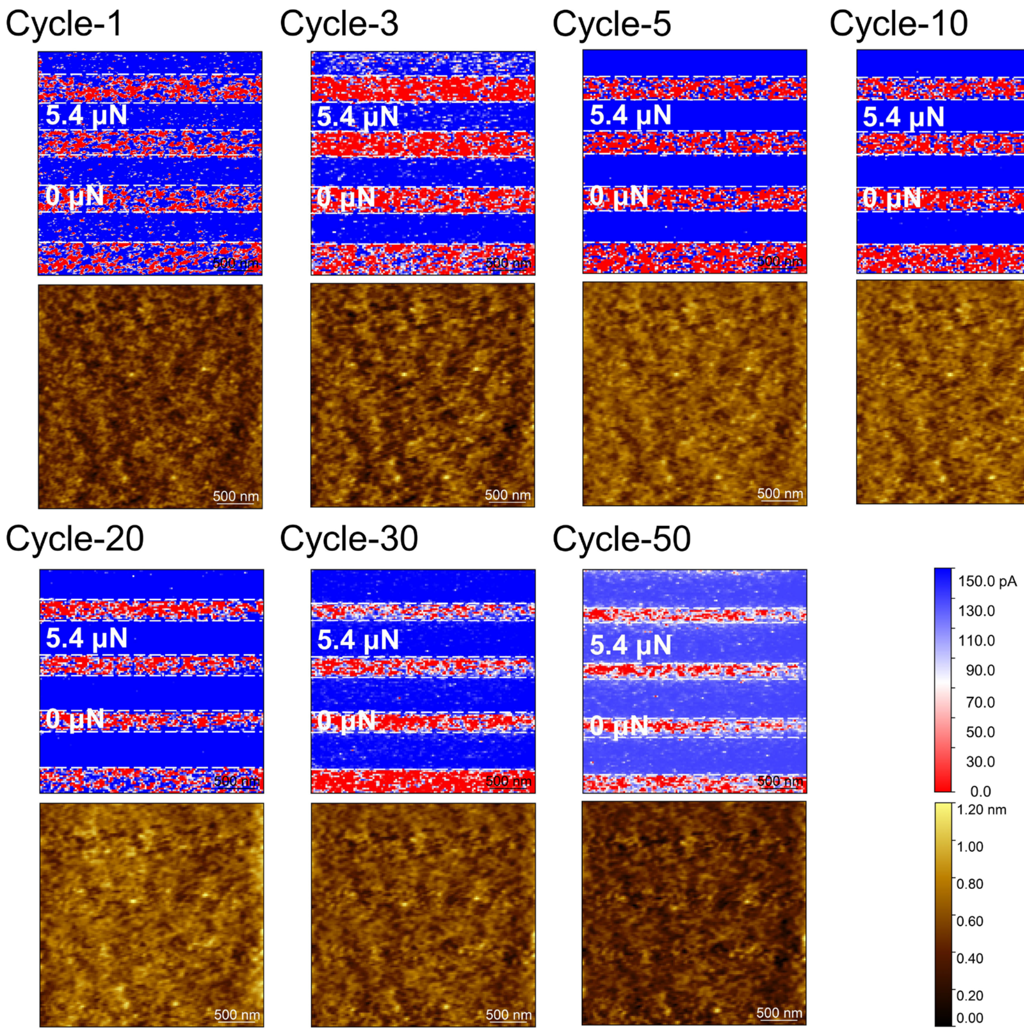

Fig.S7 Current and surface morphology after different write cycles

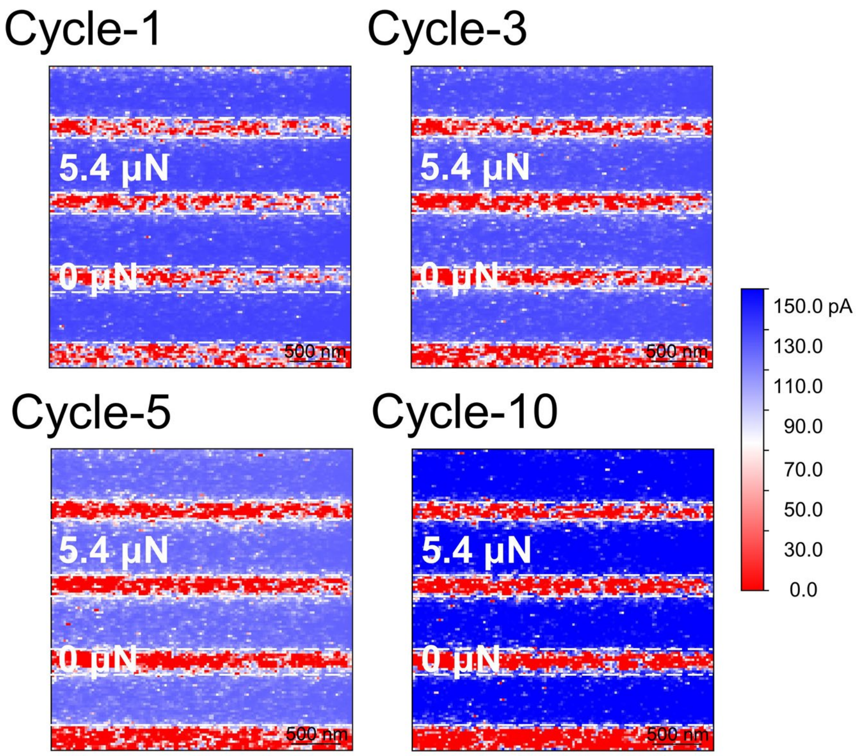

Fig.S8 Current graph after different reading cycles

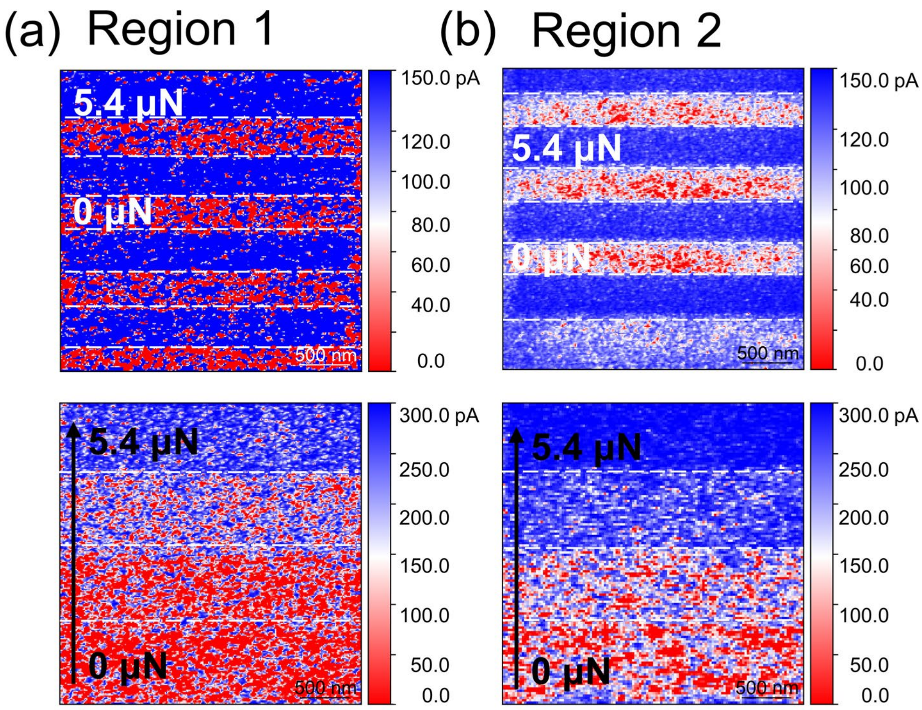

Fig.S9 Repeatability testing of resistive switching of $WO_{3-\delta}$ thin film

To confirm the repeatability of resistive switching induced by mechanical force, different region of the same sample with the manuscript (Region 1) and other sample made under the same conditions (Region 2) are selected for switching testing. The nearly identical resistance states respond to mechanical stress confirms the excellent repeatability of the $WO_{3-\delta}$ thin film.

The pressure distribution directly below the spherical indenter is[1,2,3]:

$$\frac{\sigma_z}{P_m} = -\frac{3}{2}\left(1-\frac{r^2}{a^2}\right)^{1/2} \qquad r \le a \tag{4}$$

P_m, σ_z and a are the average pressure on the contact surface, the normal pressure, and the contact radius, respectively.

The contact depth h and contact radius under the application of force F are:

$$h = \left(\frac{3F}{4E\sqrt{R}}\right)^{2/3} \tag{5}$$

$$a = \sqrt{Rh} \tag{6}$$

R and E are the radius of the indenter and the Young's modulus, respectively.

Represented by cylindrical coordinates, the stress distribution under the spherical indenter is:

$$\frac{\sigma_r}{P_m} = \frac{3}{2}\left\{\begin{matrix} \frac{1-2\vartheta}{3}\frac{a^2}{r^2}\left[1-\left(\frac{z}{U^{1/2}}\right)^3\right]+\left(\frac{z}{u^{1/2}}\right)^3\frac{a^2u}{u^2+a^2z^2}+\frac{z}{u^{1/2}} \\ \left[u\frac{1-\vartheta}{a^2+u}+(1+\vartheta)\frac{u^{1/2}}{a}tan^{-1}\left(\frac{a}{U^{1/2}}\right)-2\right] \end{matrix}\right\} \tag{7}$$

$$\frac{\sigma_\theta}{P_m} = -\frac{3}{2}\left\{\begin{matrix} \frac{1-2\vartheta}{3}\frac{a^2}{r^2}\left[1-\left(\frac{z}{u^{1/2}}\right)^3\right]+\frac{z}{u^{1/2}} \\ \left[2\vartheta+u\frac{1-\vartheta}{a^2+u}+(1+\vartheta)\frac{u^{1/2}}{a}tan^{-1}\left(\frac{a}{U^{1/2}}\right)\right] \end{matrix}\right\} \tag{8}$$

$$\frac{\sigma_z}{P_m} = -\frac{3}{2}\left(\frac{z}{u^{1/2}}\right)^3\left(\frac{a^2u}{u^2+a^2z^2}\right) \tag{9}$$

$$\frac{\tau_{rz}}{P_m} = -\frac{3}{2}\left(\frac{rz^2}{u^2+a^2z^2}\right)\left(\frac{a^2u^{1/2}}{a^2+u}\right) \tag{10}$$

$$r^2 = x^2 + y^2 \tag{11}$$

$$u = \frac{1}{2}\left[\left(r^2+z^2-a^2\right)+\left[\left(r^2+z^2-a^2\right)^2+4a^2z^2\right]^{1/2}\right] \tag{12}$$

ϑ is Poisson's ratio for materials. According to Hooke's law, the strain at this point can be expressed as:

$$\varepsilon_i = \frac{1}{E}\left[\sigma_i - \vartheta\left(\sigma_j + \sigma_k\right)\right] \tag{13}$$

$$\varepsilon_{ij} = \frac{1+\vartheta}{E}\tau_{ij} \tag{14}$$

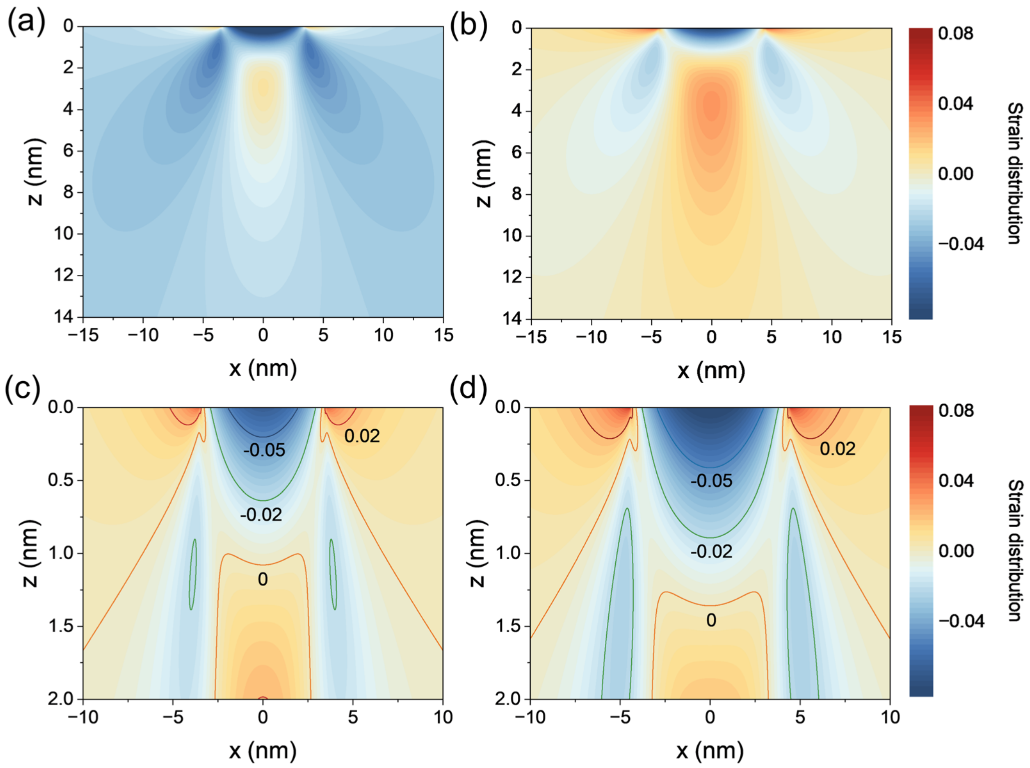

Fig.S10 (a) (b) The strain distribution of the entire film under mechanical forces of 1.8 and 3.6 μN, respectively. (c) (d) Enlarged image of the film at a depth of 2nm.

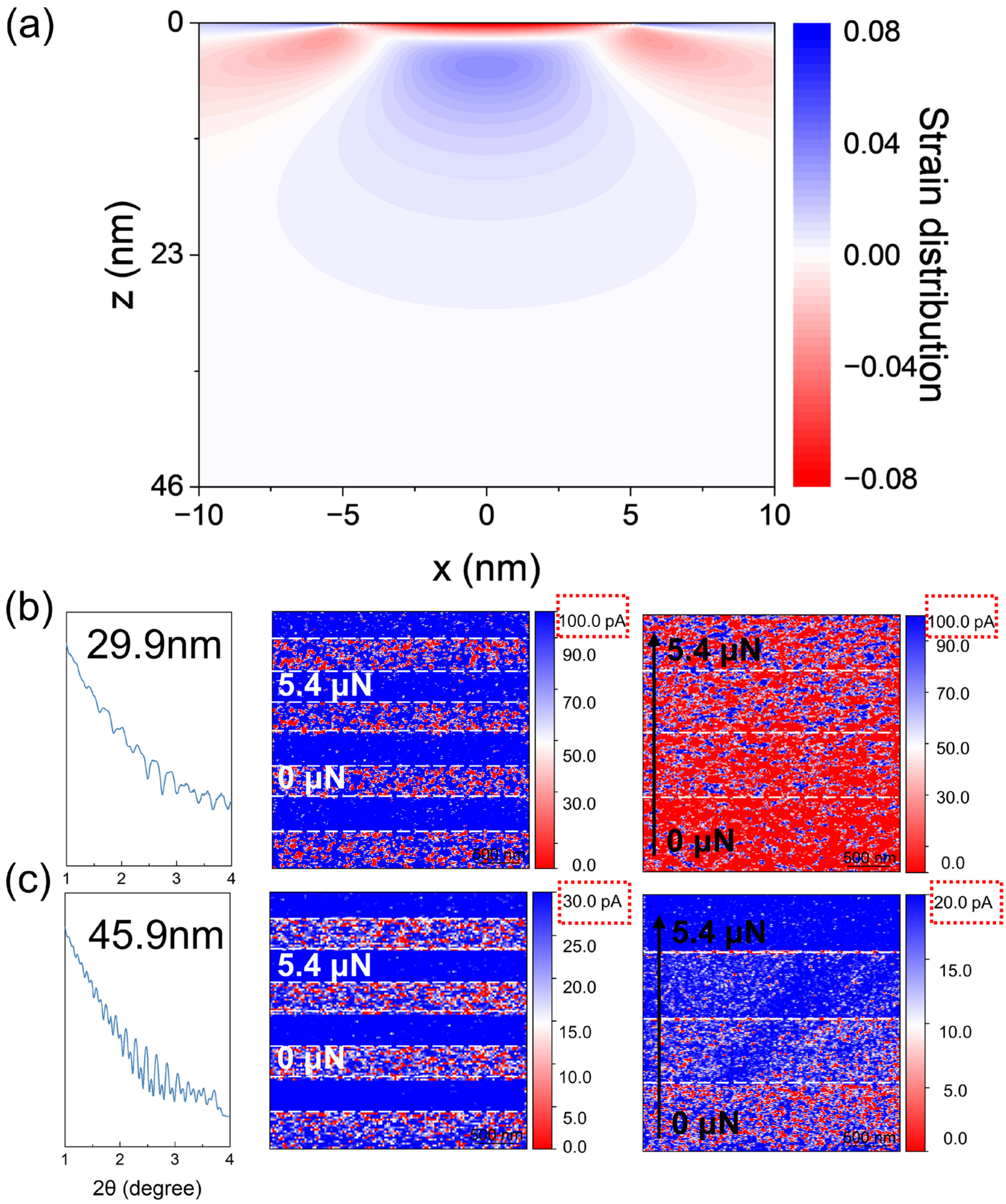

Fig.S11 (a) The strain distribution of $WO_{3-\delta}$ thin film with a thickness of 46 nm under mechanical force of 5.4 μN. (b) (c) XRR and CAFM plots with different thickness of $WO_{3-\delta}$ thin film.

As the thickness of $WO_{3-\delta}$ thin film increases, the current difference between high and low resistance states induced by mechanical force decreases. The current differential of the 45.9 nm thin film is only about 1/5 of the 13.8 nm thin film, and the range of intensity bar is also set as 1/5 in order to notice a substantial resistive switching (red dashed box of intensity bar).

Reference:

1 L. Wang, S. Liu, X. Feng, C. Zhang, L. Zhu, J. Zhai, Y. Qin and Z. L. Wang, Flexoelectronics of centrosymmetric semiconductors, *Nature Nanotechnology*, 2020, **15**, 661-667.

2 L. Dai, J. Zhao, J. Li, B. Chen, S. Zhai, Z. Xue, Z. Di, B. Feng, Y. Sun and Y. Luo, Highly heterogeneous epitaxy of flexoelectric $BaTiO_{3-\delta}$ membrane on Ge, *Nature Communications*, 2022, **13**, 2990.

3 A. C. Fischer-Cripps, *Introduction to contact mechanics*, Springer, 2007.